Geophysical Journal International

*Geophys. J. Int.* (2021) **224,** 813–824
Advance Access publication 2020 September 25
GJI Seismology

doi: 10.1093/gji/ggaa465

# Deciphering the dynamics of a heterogeneous sea cliff using ambient vibrations: case study of the Sutta-Rocca overhang (southern Corsica, France)

E. Diego Mercerat,[1] Jean Baptiste Payeur,[2] Etienne Bertrand,[1] Marie Malascrabes,[3] Michel Pernoud[1] and Yannick Chamberland[3]

[1]*Equipe MouvGS, Cerema Méditerrannée, Sophia Antipolis,* 06903, *Valbonne, France. E-mail: diego.mercerat@cerema.fr*
[2]*Département Géotechnique et Risques Naturales, CH-*3401, *Haute École Spécialisée Bernoise, Berthoud, Switzerland*
[3]*Service Risques Géologiques, Cerema Méditerrannée,* 06903, *Sophia Antipolis, France*

Accepted 2020 September 24. Received 2020 September 10; in original form 2019 December 12

## SUMMARY

We report here an interesting case study of dynamic characterization of a limestone sea cliff area, named the Sutta-Rocca overhang, located near the medieval town of Bonifacio (southern Corsica, France). The site belongs to an UNESCO protected area with an important number of visitors per year. Therefore, it is of particular interest to evaluate the potential rockfall hazard along the cliff. With the objective of evaluating the feasibility of an operational technique to monitor the cliff using ambient vibrations, two seismic stations were installed during six months (from 2016 November to 2017 April) in order to identify and monitor the resonant frequencies of the *a priori* unstable rock mass. Several techniques of classical seismic monitoring are tested on the site: single-station spectral analysis for identification of frequency peaks related to the unstable mass, relative spectral amplifications between stations and the operational modal analysis of the cliff. In particular, data analysis from a temporary campaign of two days of continuous recordings by a linear array of seismometers perpendicular to the sea cliff highlights the main characteristics of the ground motion: the overall motion of the promontory mainly in the north–south direction (perpendicular to the coast) and bending vertical and parallel to the cliff (east–west direction) at higher frequencies. The strong vertical and east–west seismic amplifications are also confirmed by the analysis of five local seismic events recorded at both semi-permanent stations. Even if ambient vibrations and seismic data analysis allows to decipher the dynamics of the Sutta-Rocca overhang, we conclude that classical seismic monitoring of just one single frequency peak with a limited number of sensors is not recommended for this particular site.

**Key words:** Instability analysis; Time-series analysis; Seismic noise; Site effects.

## 1 INTRODUCTION

Geophysical instrumentation of fractured rock masses with relatively high risk of rockfall or landslides is being performed in a number of sites presenting different sizes and environmental conditions. It has been recognized that long-term monitoring of these areas is critical for the economic development of mountainous and coastal urbanized areas. Several methodologies are proposed to monitor from geological field mapping to periodical topographical surveys (using terrestrial or airborne Laser imaging Detection and Ranging techniques, Global Navigation Satellite System positioning system and/or satellite-based imaging). These techniques have the main advantage of relatively high spatial resolution, but they are not conceived for short-term monitoring or even forecasting a potential sudden rockfall. On the other side, geophysical techniques based on ambient vibrations are increasingly used for this type of short- to mid-term (several days to years) monitoring of potential rockfall and landslides. From large-scale sites ranging from several million cubic metres (Jongmans *et al.* 2009; Gaffet *et al.* 2010; Helmstetter & Garambois 2010; Le Roux *et al.* 2011; Moore *et al.* 2011; Mainsant *et al.* 2012) to medium size rock columns (from $10^3$ to $10^5$ cubic metres) have been studied (Lévy *et al.* 2010, 2011; Bottelin *et al.* 2013b, a). All of them clearly established the feasibility of monitoring specific frequency peaks not only to assess the rockfall hazard, but also the effect of reinforcement works at some sites (Bottelin *et al.* 2017). In these studies, the analysis of Fourier spectra of ambient noise, and in some cases, the analysis of the ratio of the spectrum of horizontal-to-vertical components (HVSR) are used to

determine the vibration frequency of unstable blocks. These spectra are compared with those at sensors situated on nearby stable zones where these peaks are absent. In general, the frequencies associated with the vibration of independent blocks detached, or partially detached, from the stable massif have a polarization perpendicular to the fracture surface and present much higher frequencies relative to the vibration of the solid mass as a whole (regional vibration of the massif or the entire stratigraphic sequence).

The long-term monitoring of the evolution of the fundamental frequency informs on the state of the healthy massif—unstable block connections at the level of the discontinuity. A sharp drop in the resonant frequency can indicate a sudden rupture of rock bridges, pre-figuring the fall of the rock column. In summary, several authors agree that the method is well adapted for monitoring rock columns well separated from an intact massif (Lévy *et al.* 2011; Burjánek *et al.* 2012; Bottelin *et al.* 2013a), however, the temporal evolution of the fundamental frequency is very dependent on the temperature, which strongly complicates its monitoring as it is necessary to dissociate thermal effects (reversible) from the irreversible rock bridges breaking effects, in order to be able to predict a possible fall (Lévy *et al.* 2011; Bottelin *et al.* 2013a).

Another approach widely used in the recent literature consists in studying the distribution of frequencies in space using small aperture arrays recording simultaneously the ambient noise (Burjánek *et al.* 2010) in order to determine the link between these frequencies and regional and local fracturing of the massif. Burjánek *et al.* (2012) studied a potentially unstable rock slope in the Swiss Alps by seismic array and polarization techniques and showed the presence of standing waves (normal modes of vibration) strongly polarized perpendicular to the mapped tensional cracks at the ground surface (Lévy *et al.* 2010; Galea *et al.* 2014; Iannucci *et al.* 2018). In a recent systematic approach of 25 unstable rock slopes in the Swiss Alps by Kleinbrod *et al.* (2019), a first classification is proposed based on their dynamic behaviour: *volume-controlled* instabilities which are characterized by eigenvibrations of a clearly delimited rock mass, and *depth-controlled* instabilities which are characterized by horizontally propagating surface waves, then well suited for seismic arrays studies where dispersion characteristics can be used to image the subsurface.

Because of the geological context, our case study lies closer to recent works carried out in the Mediterranean region, more specifically in the island of Malta, where many coastal cliff sites with mapped geological instabilities and, in many cases, effective rockfalls are well documented (Panzera *et al.* 2012; Vella *et al.* 2013; Galea *et al.* 2014; Iannucci *et al.* 2018). These studies are mainly based on single station analysis (HVSR, polarization and ellipticity in function of frequency) which already gives insight on the engineering geology zonation discriminating unstable (e.g. landslides) and stable areas (limestone plateau, Iannucci *et al.* 2018). Our main objective is to evaluate, by means of seismic monitoring, the potential rockfall hazard of the Sutta-Rocca overhang, that is located in a touristical coastal area and presents similar geomorphological characteristics to other parts of the coast where rock collapses have occurred in the past. Soon after our first reconnaissance fieldwork, we realized that the dynamic characterization of the area would not be straightforward, in terms of clear identification of one or several frequency peaks to discriminate between the unstable from the stable zones. In fact, this study suggests that the previously proposed methodology is not always *ready to use*, specially when the fracture is not well exposed (or recognized) at the ground surface. In addition, we show here the importance of vertical amplifications at the site, suggesting that the vertical components of motion should not be disregarded in ambient vibration analysis, specially of rock promontories. Finally, the originality of the present case study of ambient vibration monitoring lies on the highly heterogeneous rock formations involved, bringing together geomorphological complexity and anthropogenic (yacht harbour) and natural (sea waves and strong wind) origins of ambient vibrations.

## 2 GEOMORPHOLOGY OF THE SUTTA-ROCCA OVERHANG

The cliffs of Bonifacio located at the southern tip of Corsica island, expose two stratigraphic series of shallow marine Miocene deposits: the reefal Cala di Labra Formation (upper Burdigalian) and the Bonifacio Formation (Lower Langhian). Both series are transgressive on the faulted Hercynian Basement. The Sutta-Rocca overhang is part of the Bonifacio Formation, which is composed of the Pertusato Member at the base and the Bonifacio Member at the top composed of a succession of sandstones and calcarenites over 50–80 m in thickness (André *et al.* 2011). The series is interpreted as an offshore tidal system, deposited in a slightly deep environment (from 25 to 40 m water depth). The carbonate content of the sediments increases towards the top of the Bonifacio Formation which is subdivided in four units that can be followed along the cliffs without strong lateral changes. From the bottom to the top: B1 is composed of poorly cemented calcareous litharenites with small amount of skeletal grains, unit B2 consists of calcarenites with bulk lithology of the siliciclastic grains similar to B1, and B3 is composed of cross-bedded calcarenites dominated by coralline algae. Unit B4 corresponds to a 20 m thick structureless calcareous deposit incised on top of unit B3 (Reynaud *et al.* 2013). This stratigraphic series is responsible along the coast, and especially at the Sutta-Rocca area, of the overhanging of units B2–B4. Indeed, under the mechanical action of sea waves, wind and other meteorological factors, the unit B1 of the Bonifacio Formation and the Pertusato unit P3 deteriorate, erode and thus cause the overlay of the higher series. One of the most important overhang is Sutta-Rocca, which reaches 30 m deep at the actual sea level (see Fig. 1).

The Bonifacio basin filled by the previously described sedimentary formations is carried out in a tectonic context of syn-depositional faults (Reynaud *et al.* 2013). These faults are at the origin of the actual morphology of the Bonifacio cliffs. Among them, several families have been highlighted and mapped with azimuths of N20°, N150°, N110° and N190° (Fig. 1).

According to their spatial distribution, the various fracture families identified are responsible of rockfalls from a few cubic decimetres to several thousands cubic metres. The frequency of rockfalls is higher for the small volumes, however the presence of large volume boulders at the foot of the cliff shows that these events have already occurred in the past. However, the rockfall kinematics is still poorly known in the area with several potential triggering factors. From a lithological point of view, the Bonifacio cliffs are highly heterogeneous, because even if different depositional phases were identified, the cliff is entirely constituted of finely cross-bedded lamination of layers. This heterogeneity certainly complexifies the analysis of its overall mechanical behaviour.

Specifically, behind the Sutta-Rocca overhang, a N110° vertical crack is clearly visible on the western face (Fig. 1). This crack does not seem to cut the upper calcareous layer, nor the whole of the overhang, since it has not been observed on the eastern face of the overhang. Its extension inside the rock massif remains unknown up to date. Then, the objective of this study is to test whether dynamic


**Figure 1.** (a) Location map of the study area at the southern tip of Corsica island in the Mediterranean sea. (b) Detailed aerial view with the mapped faults of the Bonifacio formation (orange dashed lines). The coastal morphology is the result of erosion combined with tectonic accidents. Zoom-on the area of the Sutta-Rocca overhang. (Aerial photo Géoportail.) (c) Sedimentary sequence of the Sutta-Rocca overhang interpreted after Reynaud *et al.* (2013). From bottom to the top, unit P3: sands of the top of Pertusato series, unit B1: calcareous and sandy layers of the Bonifacio unit (B1) and units B2–B4: reefal calcareous rocks of Bonifacio series. The vertical N110° crack is marked by the dashed black line. The colour version of this figure is only available in the electronic edition.

measurements can give insight on its extension and actual kinematic behaviour.

## 3 DATA ANALYSIS

### 3.1 Spectral analysis of linear array data

One temporary campaign took place during 2016 October 11 and 12. It consisted of a linear array of 10 seismic stations equipped by three components Lennartz (Le3D, 5 s) seismometers all plugged to a CityShark II (LEAS) digitizer recording at 200 Hz sampling frequency. The objective was to study a complete north–south profile going from the Sutta-Rocca overhang (station 01 in the map of Fig. 2) to the yacht harbour side (station 10) to identify the possible unstable areas with marked frequency peaks. Two arrays of six stations at a time were used repeating location 05 and 06 to have two control (reference) points. The recording time of each array was 4 hr for the linear array 1 October 11 and 3 hr for the linear array 2 of October 12. It has to be noted that different meteorological conditions occurred during these days (relative calm weather on October 12, whereas more windy weather on October 11).

The spectral analysis of both arrays has been done using the geopsy package (Wathelet *et al.* 2020) with a Konno & Ohmachi (1998) smoothing ($b = 40$) used for each spectrum, is summarized in Fig. 3. It shows several peaks in the frequency band between 1 and 15 Hz for all stations which, at the first glance, make quite difficult the association of one particular peak to the relative motion of the Sutta-Rocca overhang. In fact, as we will shortly see, the hypothesis of a clear discontinuity (vertical fracture) separating the overhang from the rest of the massif is disadvantaged after the present analysis. In order to normalize the power spectral densities (PSDs), using the two colocated stations 05 and 06, we apply the

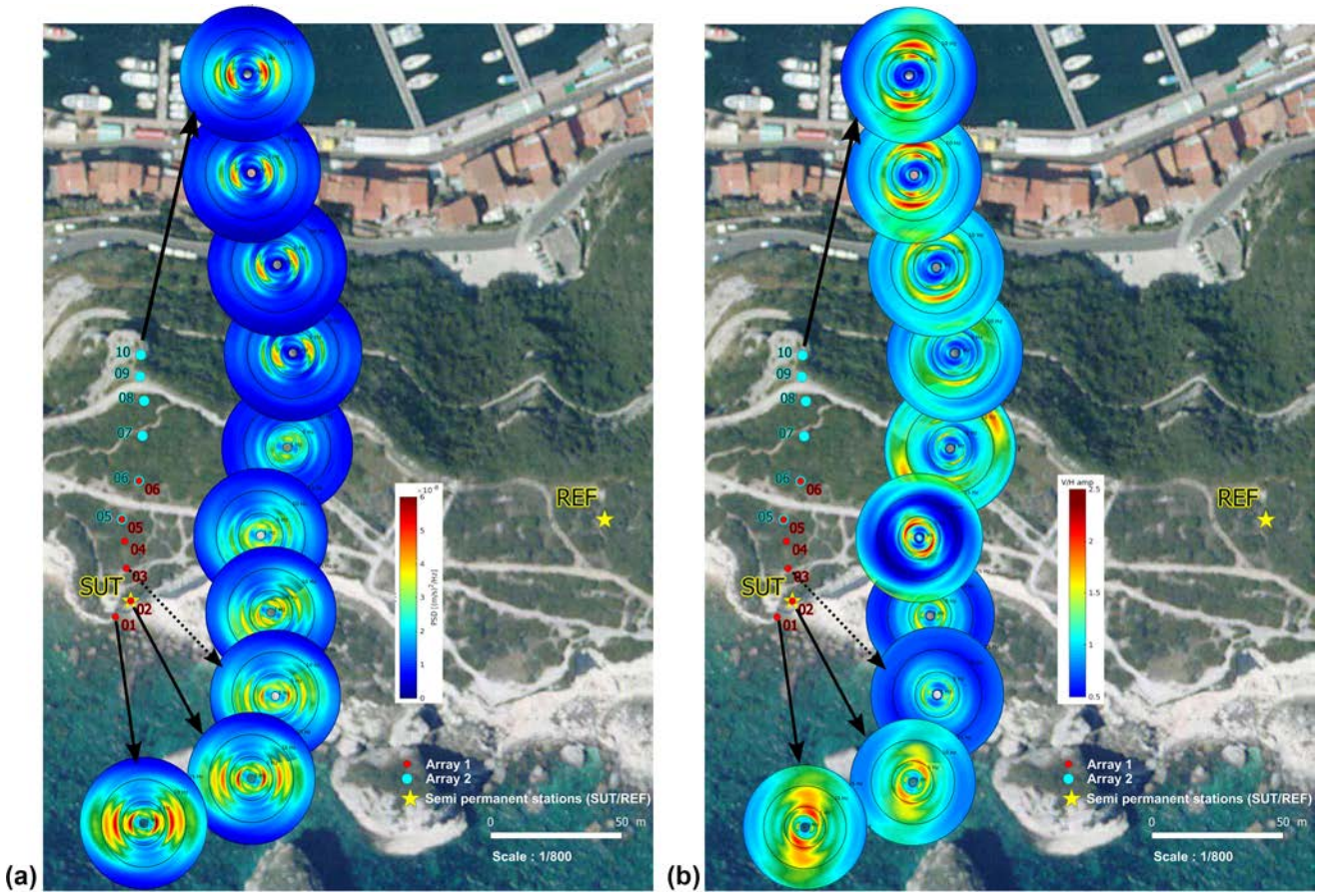


**Figure 2.** Temporary linear arrays 1 and 2 across the Bonifacio promontory. Stations 01 and 02 (SUT) are located on top of the Sutta-Rocca overhang. (a) The coloured polar plots show the horizontal PSD calculated from 3 hr of ambient vibrations. Frequency along the radius from 1 to 15 Hz. (b) Idem for the VHSR. The colour version of this figure is only available in the electronic edition.

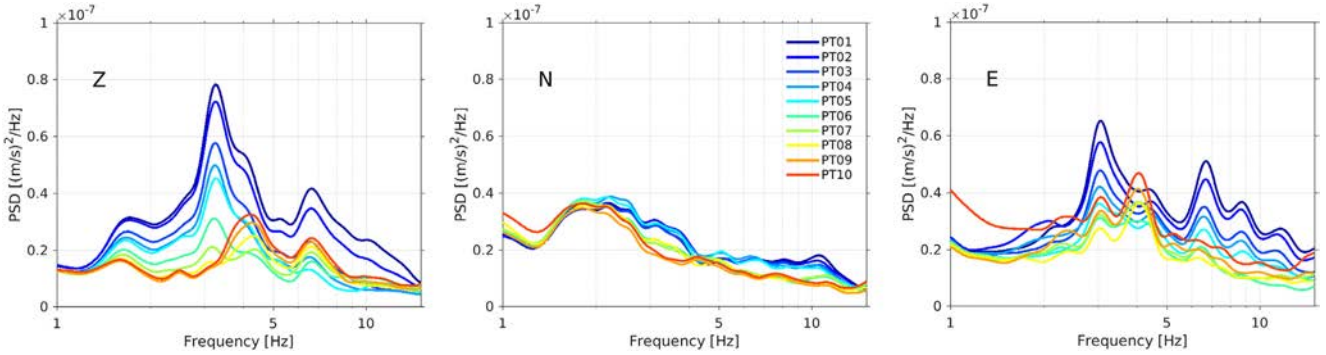


**Figure 3.** Mean PSD of 3 hr of ambient vibrations in the three components of stations 01 (seaside) to 10 (harbour side). Renormalization applied to mean PSDs of stations 01 to 06 (windy weather). The colour version of this figure is only available in the electronic edition.

following frequency-dependent factor to the spectra corresponding to the windy day,

$$\mathrm{norm}_i(f) = 0.5\left(\frac{\mathrm{FFT}_i(05)_{\mathrm{wind}}}{\mathrm{FFT}_i(05)_{\mathrm{calm}}} + \frac{\mathrm{FFT}_i(06)_{\mathrm{wind}}}{\mathrm{FFT}_i(06)_{\mathrm{calm}}}\right), \quad (1)$$

where $\mathrm{FFT}_i(.)$ corresponds to the Fourier spectra of each component $i = Z$, $N$ and $E$.

From the PSDs calculated from 3 hr of data for each profile summarized for all stations in Fig. 3 (for each separated spectrum see Figs A1 and A2 in Appendix A) several features can be observed: (a) four picks are present at almost all stations around 1.7, 3.1, 4.3 and 6.6 Hz; (b) besides the clear difference on noise power between the two set-ups, the first two spectral picks are better expressed in the stations close to the seaside (01–05) and the latter two in the northern stations close to the yacht harbour (06–10) and (c) except for the first peak at 1.7 Hz, all other picks are better expressed in the vertical and the east–west components, instead of the north–south direction (Fig. 3). This is somehow counterintuitive regarding the main fracture orientation (N110°) described in the previous section, which may indicate that the fracture is not expressed in the upper geological units. Fig. 2 shows the PSDs of the horizontal components and their distribution along the profile. The highlighted peaks can

be followed all along the profile with slight differences in amplitude and azimuth, but showing the same general pattern. On the other side, the analysis of Fig. 3 put forward the large spectral power in the vertical direction with respect to the horizontal ones. Finally, we stress that the PSDs noise levels in all three components lie in between the NHNM and NLNM models of Peterson (1993), that is around $10^{-7}$ and $10^{-9}(\mathrm{m\,s^{-1}})^2\,\mathrm{Hz}^{-1}$, respectively, in the frequency band of interest here.

Another single-station approach to analyse ambient vibration data consists of the study of HVSRs. The technique has been successfully applied by Panzera *et al.* (2012) and Iannucci *et al.* (2018) to discriminate between stable and unstable areas on the limestone cliffs of the island of Malta. In the case of Sutta-Rocca overhang, unfortunately, there is no straightforward relation between the sensors on the overhang (01 and 02) and the presence or absence of peaks. Mainly because both horizontal components do not show marked frequency peaks in the raw Fourier spectra as can be seen in Fig. 3. Moreover, the presence of strong peaks in the vertical component, at frequencies where also the east–west component is important, precludes any interpretation in terms of Rayleigh wave ellipticity or 1-D-*SH* resonance, favouring instead a kind of structural vibrational modes at those frequencies (Burjánek *et al.* 2012; Panzera *et al.* 2012). On the contrary, interesting information can be extracted from the inverse of HVSR amplitude, that is the vertical-to-horizontal spectral ratio (VHSR), as the largest spectral amplitudes are found in the vertical component. In Fig. 2 for example, the azimuthal VHSR ratios are shown all along the profile. The main vertical amplifications are essentially aligned in the NS direction (perpendicular to the cliff) suggesting a sort of cantilever beam behaviour with marked flexural modes. These frequency peaks will be analysed in the following section using a multisensor technique.

### 3.2 Operational modal analysis of linear array data

In order to thoroughly analyse the continuous data acquired along the seismic profile, we decide to apply an operational modal analysis (OMA) to the ambient vibration recordings. Doing so, we expect to capture the dynamic behaviour of the overhang area. This technique has been widely used in mechanical and structural engineering to identify modal parameters (frequencies, damping and modal shapes) of linear systems from *output-only* measurements such as systems excited by ambient vibrations. Among the different OMA methodologies, most of the applications are based on the frequency-domain decomposition (FDD) technique (Brincker *et al.* 2001). It basically relies on the singular value decomposition of the signals cross-PSD matrix to retrieve the eigenfunctions of the mechanical system. For details about the technique, the reader may refer to the thorough review by Brincker (2014). The technique assumes input loads presenting white noise characteristics in the frequency bandwidth of interest. In the last decade, it has been applied to different geological structures, such as the characterization of 1-D soil column responses from borehole measurements (Gueguen *et al.* 2011) and across basin structures with 2-D geometries (Ermert *et al.* 2014; Poggi *et al.* 2014). Bottelin *et al.* (2013b) applied OMA to an ustable rock column with just three seismometers using the FDD technique. More recently, Häusler *et al.* (2019) applied the technique to successfully image a fracture network in an unstable slope in the Swiss Alps. The study not only confirms the previously identified frequencies at the site by Burjánek *et al.* (2012), but also adds information about higher modes that were not interpreted beforehand (Häusler *et al.* 2019).

The identification procedure used in this work is also based on the FDD technique. Once a particular resonant frequency is identified by the maximum in the cross-power spectral matrix, the corresponding eigenvector is extracted and interpreted as representative of the modal shape of the system at that frequency. The technique allows in a sense to consider not only the amplitude but also the relative phase differences between sensors of the array and therefore to visualize relative displacements between them.

After calculation of the eigenvalues of the cross-spectral matrix, the technique needs the definition of a reference channel for modal shape normalization. Its modal amplitude is set to one for every set-up, and all other relative displacement are calculated with respect to this value. The vertical component of 05 is used as reference channel to assemble both data sets and produce modal shapes for the whole stations profile. The FDD analysis is performed with the help of the MACity software (Michel 2007; Michel & Guéguen 2010). After some tests using different spectral resolutions for the calculation of the cross-spectral matrix, time windows of 10.42 s of duration (frequency resolution of $\Delta f = 0.096$ Hz) with an overlap of 50 per cent seems to be a good compromise between spectral resolution and total signal length (3 hr for each set-up). The results are summarized in Fig. 4 where the first five singular values are shown. The first mode around 1.7 Hz expresses a clear N-S component as well as an important vertical motion, specially at the seaside part. From the modal shape analysis, we interpret this mode as the motion of the whole promontory in the direction perpendicular to the coast. The next identified mode around 3.1 Hz shows a relatively important E-W motion also associated with a strong vertical motion. These two first modes correspond to the main peaks already observed in the single station analysis shown in Fig. 3. After these two principal modes, some higher order modes are identified at 4.3 and 5.3 Hz. These two modes present quite similar modal shapes along the profile, though their modal assurance criterion (MAC) is quite different[1] (lower than 80 per cent). Further analysis using longer time series and higher number of sensors must be done to better identify their modal shapes. Similarly, damping coefficients may be obtained from the FDD analysis when spectral peaks are clearly identified. Regarding the limited amount of data available, this is out the scope of this study. The last identified mode around 6.6 Hz presents again a clear E-W component and an antisymmetric motion in the vertical component. Actually, all these three modes at 4.3, 5.3 and 6.6 Hz show the same feature of changing sign in the vertical direction near the central part of the promontory. As there no visible fracture or fault scarp in the area, we believe that this behaviour is related to the free movement of a kind of cantilever beam clamped at the central part of the cliff. To summarize, three main observations can be done after this multisensor analysis: (1) there is a strong vertical motion of the whole promontory for frequencies ranging from 1.7 to 6.6 Hz, with a secondary preferential E-W direction of motion (parallel to the cliff) specially at higher frequencies ($>3$ Hz), (2) the only mode with significant N-S direction (perpendicular to the cliff) is the first one at 1.7 Hz and (3) there is no evidence of a localized motion of the Sutta-Rocca overhang (stations 01 and 02) with respect to the rest of the massif, at least for the analysed frequency range.

[1]The MAC is calculated as the normalized scalar product of two vectors corresponding to mode shapes. A threshold of 70–80 per cent is generally used to consider similar mode shapes.

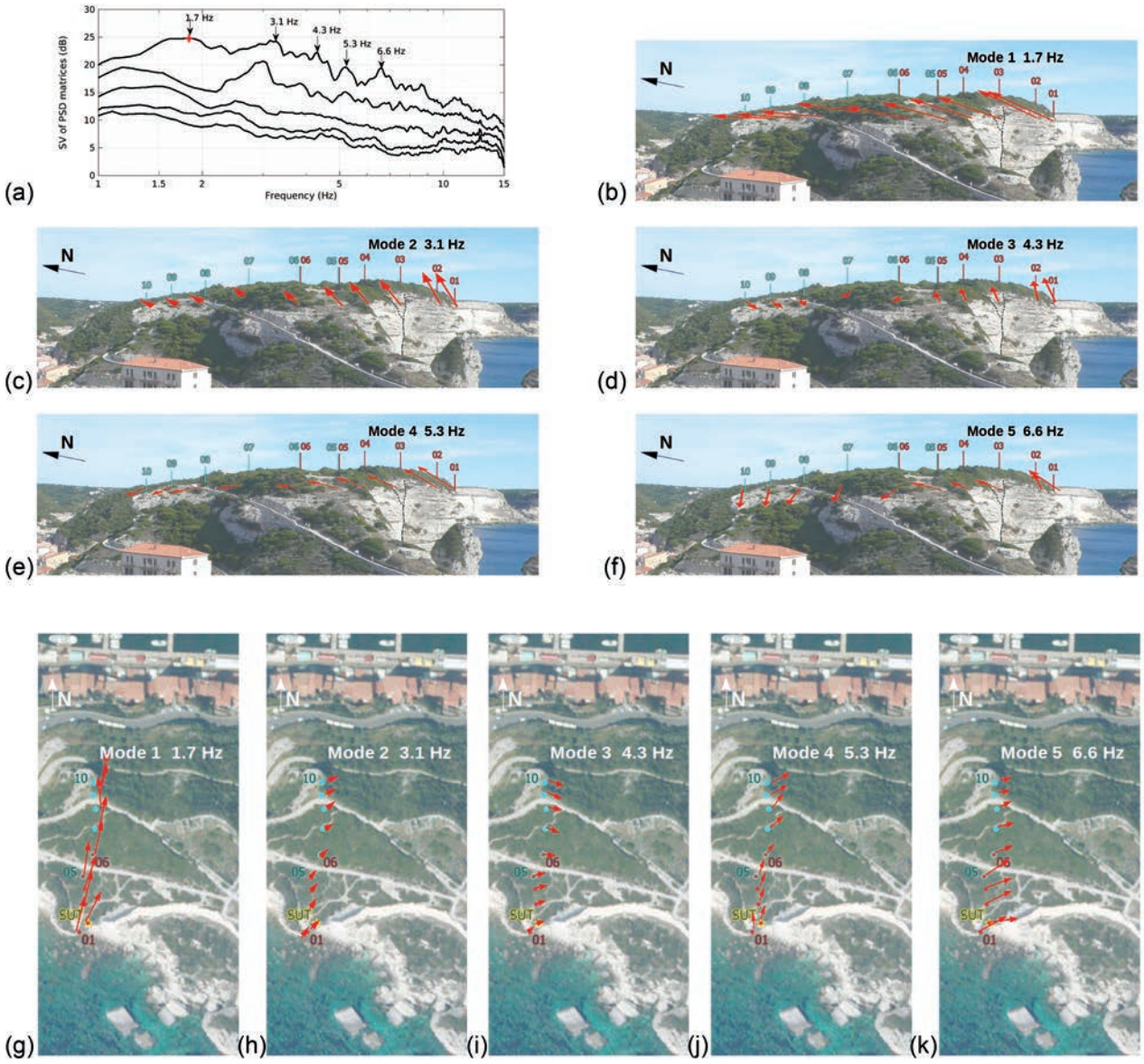


**Figure 4.** (a) First five eigenvalues of the Singular Value Decomposition decomposition of the cross-correlation matrix. Identified modal frequencies are marked with vertical arrows. (b)–(f) NS profile (view from the west) of the five modal shapes identified from the FDD analysis of 4 hr of ambient vibrations. Red arrows indicate the relative displacements corresponding to each modal shape. The position of the vertical N110° crack is shown by a dashed black line. (g)–(k) Plan views of the same modal shapes. Note that, in each figure, the absolute values of the modal shape displacements are exaggerated just for plotting purposes. The colour version of this figure is only available in the electronic edition.

### 3.3 Semi-permanent stations

From the previous analysis, there is no evident association of one frequency peak in the recorded PSD to a particular motion of the Sutta-Rocca overhang with respect to the rest of the massif. On the other side, all spectral peaks seem to be related to particular motions of the whole promontory, or at least the upper stiff calcareous layer (see Section 2). This fact also warns us about a quick interpretation of one (or some) of these peaks as strictly related to the stability of the Sutta-Rocca overhang.

Just after the temporary campaign of 2016 October, two stations were installed at the site during 6 months from 2016 November to 2017 April to record ambient vibrations continuously. One of them is located at the site of 02 of the previous linear array (at the edge of the cliff on top of the overhang, station named SUT hereafter) and the other one is located on a stable area 250 m away to the east from the Sutta-Rocca overhang (station REF hereafter). Both locations are shown with yellow stars in Fig. 2. In Fig. 5, the rotational PSD of 1 hr data from 2016 November 10, is shown for both SUT and REF stations. It is important to remark that it corresponds to a rather windy weather on the area as it will be shown later. A similar polar figure for a calm day (2016 November 27) shows a different pattern at station SUT, other than the expected lower amplitude level (note the differences in colour scale on Fig. 5. Three main features emerge from Fig. 5: (1) the pick at 1.7 Hz is seen on both stations, confirming the general motion of the whole promontory with an N-S azimuth even at 250 m away from the overhang area, (2) the pick around 3 Hz and azimuth around N120° is just seen in SUT station what suggests that it corresponds to the particular motion of the stiff calcareous layer on the overhang area in direction parallel

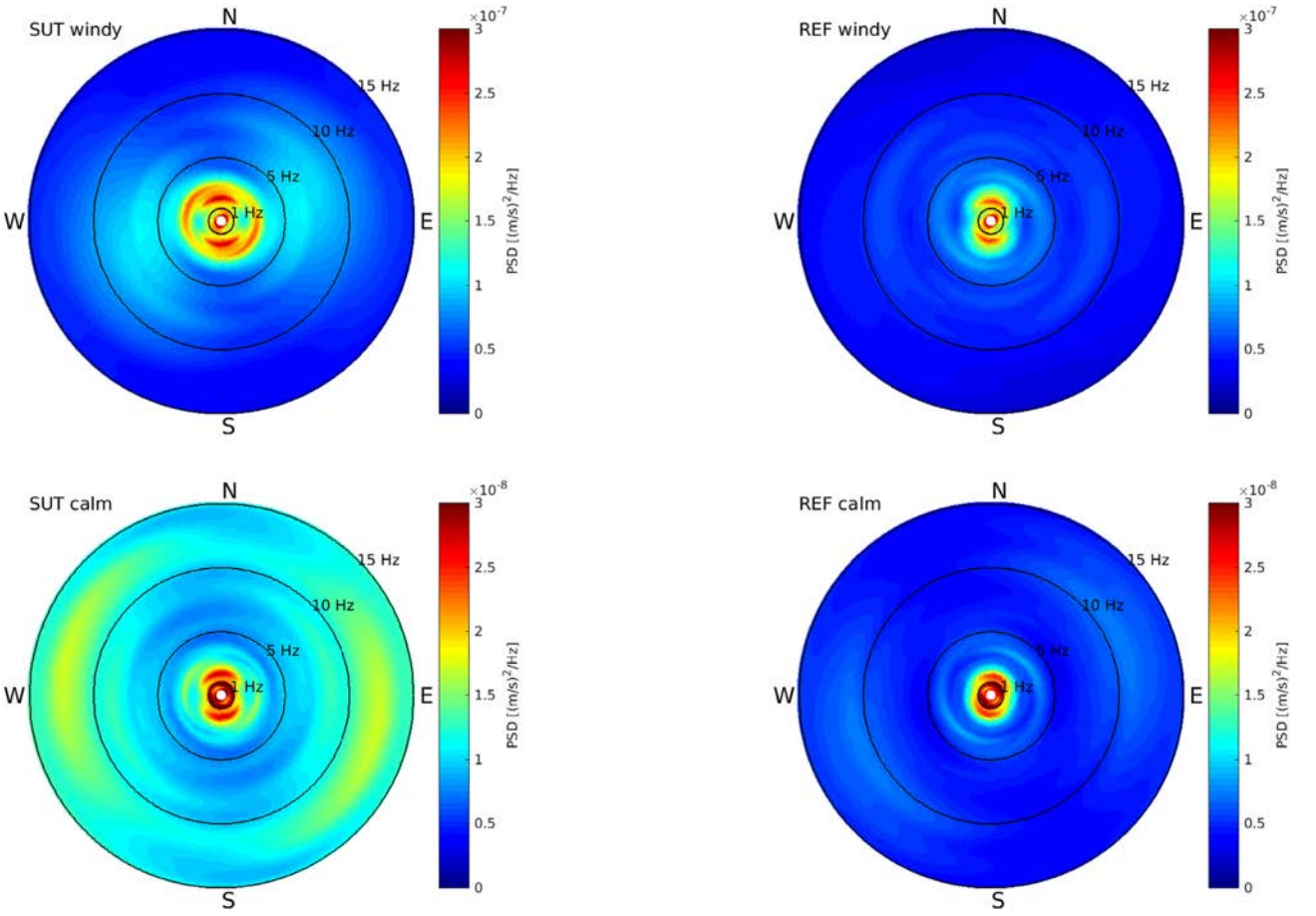


**Figure 5.** PSD of one hour ambient vibrations on windy (top) and calm (bottom) weather at SUT (left-hand column) and REF (right-hand column) stations. Note the differences in colour scale for windy and calm days. The colour version of this figure is only available in the electronic edition.

to the cliff and therefore to the pressumed crack azimuth (N110°) and (3) higher frequency peaks between 6 and 15 Hz can be seen in SUT station with again preferential E-W motion (from N70° to N110°).

### 3.4 Analysis of local seismicity recordings

During the deployment of the semi-permanent stations, few seismic events with local magnitudes around ML 3 have been recorded by both stations (see Fig. 6 for location and Table 1 for earthquake characteristics). Two examples of the recorded waveforms can be seen in Fig. 7. After Fourier transform, smoothing (Konno-Ohmachi with $b = 40$) and calculation of the Standard Spectral Ratio (SSR) between SUT and REF stations, the seismic amplifications following the three components of motion are shown in Fig. 8. Not surprinsingly, the vertical amplifications are important at several frequency peaks near 3 Hz, 5.5 Hz and 10 Hz. In fact the highest values (between 5 and 10) are found in the vertical direction around 3 Hz to 3.5 Hz. In addition, the amplification in the EW component is also important at these frequency peaks, and there is not significant amplification in the NS component. These results confirm the main motion characteristics of the Sutta-Rocca overhang deduced from the ambient vibration analysis discussed in the previous sections.

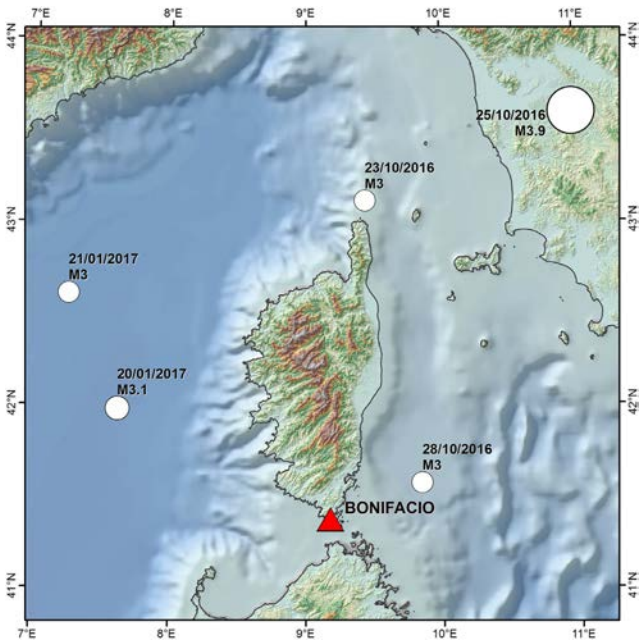


**Figure 6.** Epicentral location of the local earthquakes recorded by the semi-permanent stations and used in this study. The white circles are proportional to local ML magnitude.

**Table 1.** Earthquake used in the analysis (source EMSC).

| Date | Time UTC | Latitude (N) | Longitude (E) | Depth (km) | Magnitude | Region name |
|---|---|---|---|---|---|---|
| 2017-01-21 | 18:28:17 | 42.61 | 7.25 | 10 | ML 3.0 | Western Mediterranean Sea |
| 2017-01-20 | 03:48:08 | 41.98 | 7.62 | 10 | ML 3.1 | Western Mediterranean Sea |
| 2016-10-28 | 06:39:45 | 41.58 | 9.85 | 5 | ML 3.0 | Corsica, France |
| 2016-10-25 | 16:53:00 | 43.60 | 10.99 | 9 | ML 3.9 | Central Italy |
| 2016-10-23 | 08:18:50 | 43.12 | 9.44 | 5 | ML 3.0 | Ligurian Sea |

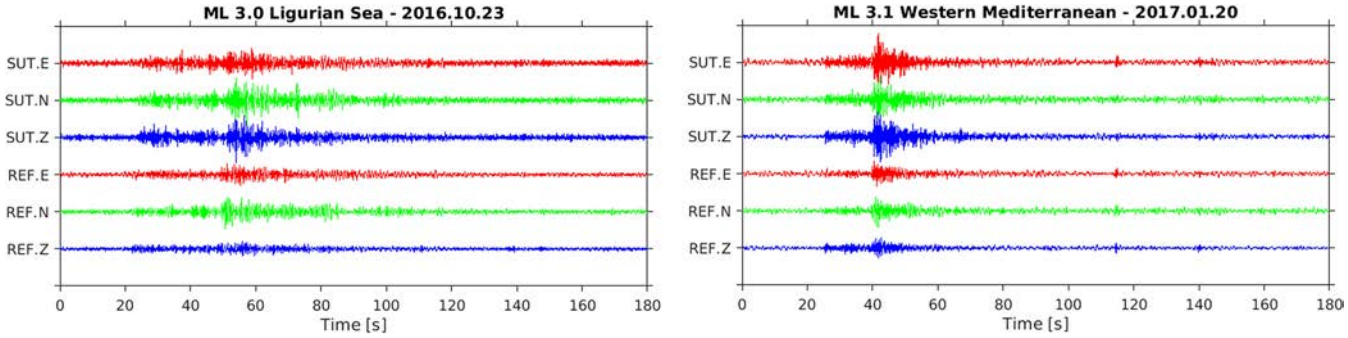


**Figure 7.** Waveforms of two local earthquakes recorded at stations SUT (sea cliff) and REF (inland).

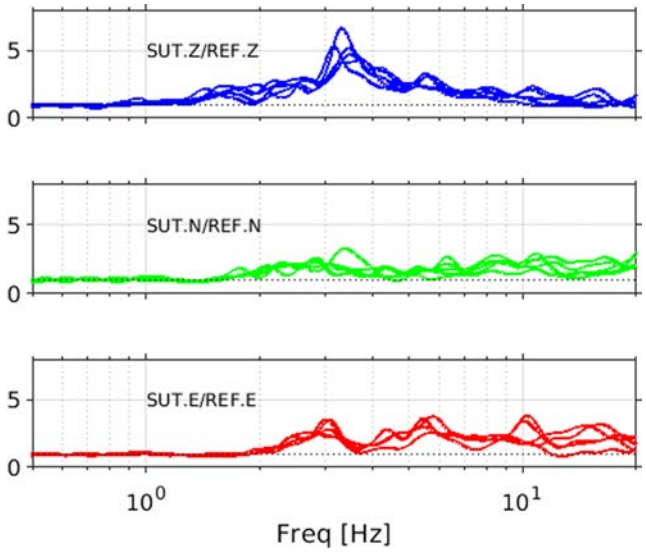


**Figure 8.** SSR between SUT and REF stations in the three directions of motion. One curve per seismic event.

### 3.5 Analysis of continuous ambient vibration recordings

Additionally, even if it is out of the scope of the present study, we briefly analyse the continuous data recorded by both stations during the whole 6 months period. Ambient vibration data are divided in 1-hr time windows from where the Fourier transform of each component are calculated (an antitriggering procedure is used to avoid local seismicity and/or wind bursts in the data). Then, SSR are calculated between SUT and REF station for each component using 1-hr length windows with a detrend and also Konno-Ohmachi smoothing before calculating the ratio. From Fig. 9, we clearly observe that the spectral peaks correspond fairly well with the previous results from local seismicity recordings. High amplifications at SUT with respect to REF are found at 3 and 5.5 Hz and between 8 and 10 Hz in the vertical component, and at 3 Hz and around 6 Hz in the E-W component (parallel to the cliff). The N-S component (perpendicular to the cliff) is not significantly amplified. There is also a clear 'comb' like pattern with a daily period, that may be related to daily temperature cycles and/or some kind of anthropogenic forcing of ambient vibrations surely generated from the harbour activity. Strikingly, this effect disapears when high wind speed ($> 40$ km h$^{-1}$) are recorded in the nearby meteorological station of Pertusato, located at 2 km to the southeast of the Sutta-Rocca overhang. It seems that high wind speeds, also related to strong wind-generated waves, is the environmental factor that influences the most the overhang motion with respect to the rest of the massif. A detailed analysis of the continuous data set will follow in future research.

## 4 DISCUSSION AND CONCLUSION

Even if the first objective of the present study, namely finding the resonant frequency of the potentially unstable Sutta-Rocca overhang, have not been satisfactory reached, many interesting features regarding the dynamics of the overhang area have been highlighted. At the same time, we have also put forward some difficulties that the operational methodology based on seismic monitoring might encounter in this type of complex environment: an heterogeneous sea cliff, close to an urbanized area, including an active yacht harbour less than 100 m downslope.

From classical Fourier spectral analysis, we emphasize how meteorological conditions affect the PSD levels recorded at each station of the linear profile. The relative amount of low-frequency content in the data drastically increases with windy weather. This may not be favourable for a clear peak reconnaissance, specially at higher frequencies that may become masked by the low frequency content related to wind. Installation conditions were not optimal: sensors at the free surface, inside holes of just few centimetres deep to avoid wind effects and assure sufficient ground coupling. In short-term seismic array measurements, the trade-off between expeditive sensor deployments and satisfactory ground coupling is unavoidable.

One way to normalize single stations measurements could be the H/V (or V/H) spectral ratios, admitting that noise sources illuminate equally the three components of motion. Anyway the use of this single-station analysis is only prone for clear *volume-based* instabilities where the spatial limits of the unstable volume are clearly seen (Galea *et al.* 2014; Iannucci *et al.* 2018; Kleinbrod *et al.* 2019).

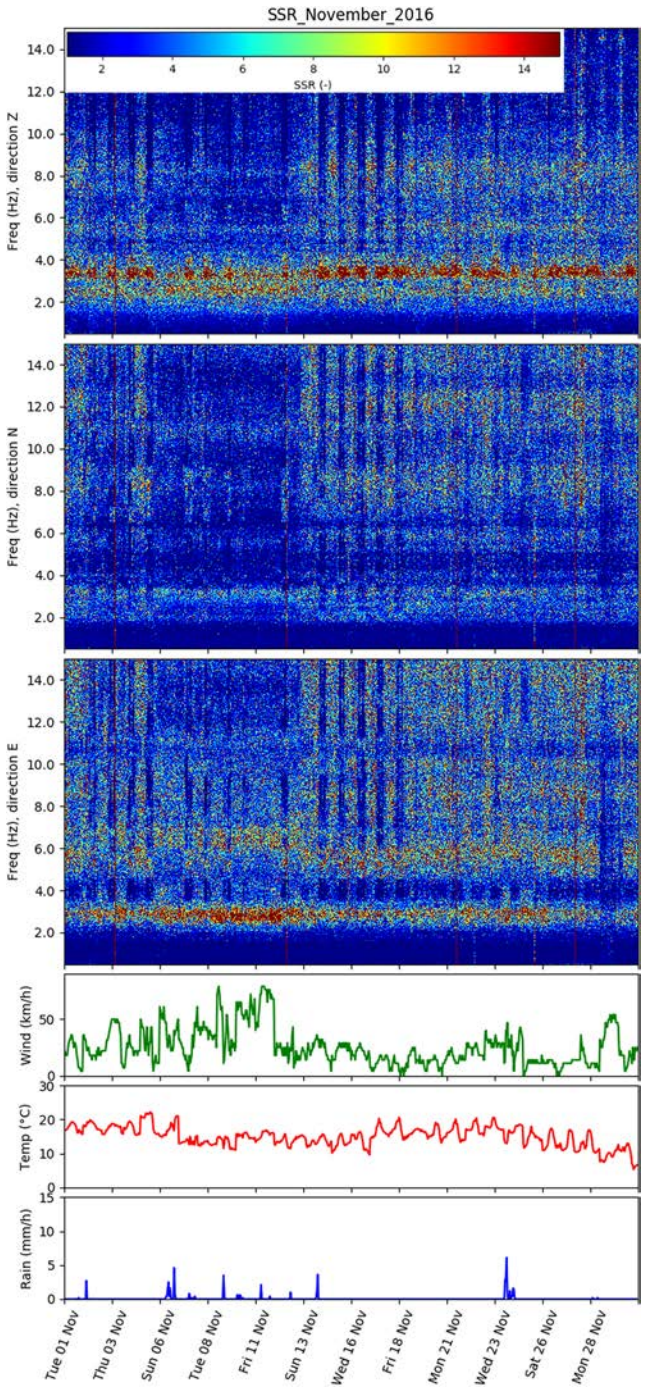


**Figure 9.** Hourly SSR between SUT and REF stations during November 2016. Meteorological parameters (wind speed, temperature and rainfall) are also shown at the bottom during the same time period. The colour version of this figure is only available in the electronic edition.

Appart from that, the HVSR curve averages out the azimuthal information that may be highly valuable when dealing with complex geological sites. Even if this ratio offers valuable information in some cases, the ability to image peculiar behaviour is still argued in the literature and therefore we prevent its use for the present case study. On the other side, the VHSR may give valuable information, at least to localize the frequency peaks of the main modes of deformation of the sea cliff.

Regarding the use of ambient vibrations analysis by FDD, the main advantage is the use of all recordings at once (via the cross-spectral density matrix) what gives reliable relative motions between stations in space. This allows to identify preferential modes of vibration that could hardly be observed from more classical single-station techniques, such as Fourier spectral peaks and/or SSR between just pair of stations. For example in the case of Sutta-Rocca overhang, the modes around 5.3 and 6.6 Hz could not have been recognized solely from single-station spectral analysis. This has also been observed by the recent work of Häusler *et al.* (2019) where a complex fracture network is imaged using the relative displacement between different rock compartments. The analysis of the first five eigenmodes have not evidenced any localized motion, suggesting the presence of higher modes of a continuous beam- or shell-like structure. In order to go one step further, a 3-D spatial array, or at least a 2-D one covering the promontory free surface, may be used to overcome the difficulties in eigenmode interpretation.

From the local earthquake analysis, we confirm the previous preferential orientations of ground motion obtained from ambient vibration analysis (i.e. important vertical and east–west amplifications). This comforts the assumption of a relatively rigid plate or shell-type behaviour of the whole promontory (particularly, the top limestone layer corresponding to units B2 to B4 of the Bonifacio Member) with an important vertical flexion as the main dynamic feature of the sea cliff area as it is shown in Fig. 4.

Finally, based on a future geomechanical modelization of the Sutta-Rocca overhang, and after clear identification of the modal shapes of the whole promontory area, the long-term monitoring could be a solution for the assessment of rockfall hazard, but surely considering many more parameters (i.e. several modal shapes, their frequencies, and, if possible, their damping coefficients) than a single resonant frequency of the potentially unstable Sutta-Rocca overhang.

## ACKNOWLEDGEMENTS

We acknowledge the remarks from two anonymous reviewers that greatly improve the quality of the final version of the paper. We also thank Jenny Trevisan (Géoazur, Univ. Côte d'Azur, France) for assistance with Fig. 6. Data processing has been done using Geopsy package (Wathelet *et al.* 2020) and MACity software (Michel 2007).

## REFERENCES

André, J.-P., Barthet, Y., Ferrandini, M., Ferrandini, J., Reynaud, J.-Y. & Tessier, B., 2011. The Bonifacio formation (Miocene of Corsica): transition from a wave- to tide-dominated coastal system in mixed carbonate-siliciclastic setting, *Bull. Soc. géol. France,* **182**(3), 221–230.

Bottelin, P., *et al.*, 2013a. Spectral analysis of prone-to-fall rock compartments using ambient vibrationscontinuous spectral analysis of unstable rock compartments, *J. Environ. Eng. Geophys.,* **18**(4), 205–217.

Bottelin, P., Lévy, C., Baillet, L., Jongmans, D. & Gueguen, P., 2013b. Modal and thermal analysis of Les Arches unstable rock column (Vercors massif, French Alps), *Geophys. J. Int.,* **194**(2), 849–858.

Bottelin, P., Baillet, L., Larose, E., Jongmans, D., Hantz, D., Brenguier, O., Cadet, H. & Helmstetter, A., 2017. Monitoring rock reinforcement works with ambient vibrations: La Bourne case study (Vercors, France), *Eng. Geol.,* **226,** 136–145.

Brincker, R., 2014, Some Elements of Operational Modal Analysis, *Shock and Vibration ,* **2014,** Article ID 325839, doi.org/10.1155/2014/325839.

Brincker, R., Zhang, L. & Andersen, P., 2001. Modal identification of output-only systems using frequency domain decomposition, *Smart Mater. Struct.,* **10**(3), 441–445.

Burjánek, J., Gassner-Stamm, G., Poggi, V., Moore, J.R. & Fäh, D., 2010. Ambient vibration analysis of an unstable mountain slope, *Geophys. J. Int.,* **180**(2), 820–828.

Burjánek, J., Moore, J.R., Yugsi Molina, F.X. & Fäh, D., 2012. Instrumental evidence of normal mode rock slope vibration: evidence of normal mode rock slope vibration, *Geophys. J. Int.,* **188**(2), 559–569.

Ermert, L., Poggi, V., Burjánek, J. & Fäh, D., 2014. Fundamental and higher two-dimensional resonance modes of an Alpine valley, *Geophys. J. Int.,* **198**(2), 795–811.

Gaffet, S., Guglielmi, Y., Cappa, F., Pambrun, C., Monfret, T. & Amitrano, D., 2010. Use of the simultaneous seismic, GPS and meteorological monitoring for the characterization of a large unstable mountain slope in the southern French Alps: microseismic and GPS survey of unstable slope, *Geophys. J. Int.,* **182**(3), 1395–1410.

Galea, P., D'Amico, S. & Farrugia, D., 2014. Dynamic characteristics of an active coastal spreading area using ambient noise measurements—Anchor Bay, Malta, *Geophys. J. Int.,* **199**(2), 1166–1175.

Gueguen, P., Langlais, M., Foray, P., Rousseau, C. & Maury, J., 2011. A natural seismic isolating system: the buried Mangrove effects, *Bull. seism. Soc. Am.,* **101**(3), 1073–1080.

Häusler, M., Michel, C., Burjánek, J. & Fäh, D., 2019. Fracture network imaging on rock slope instabilities using resonance mode analysis, *Geophys. Res. Lett.,* **46,** 12, doi.org/10.1029/2019GL083201.

Helmstetter, A. & Garambois, S., 2010. Seismic monitoring of Séchilienne rockslide (French Alps): analysis of seismic signals and their correlation with rainfalls, *J. geophys. Res.,* **115**(F3), 10.1029/2009JF001532.

Iannucci, R., Martino, S., Paciello, A., D'Amico, S. & Galea, P., 2018. Engineering geological zonation of a complex landslide system through seismic ambient noise measurements at the Selmun Promontory (Malta), *Geophys. J. Int.,* **213**(2), 1146–1161.

Jongmans, D., Bièvre, G., Renalier, F., Schwartz, S., Beaurez, N. & Orengo, Y., 2009. Geophysical investigation of a large landslide in glaciolacustrine clays in the Trièves area (French Alps), *Eng. Geol.,* **109**(1–2), 45–56.

Kleinbrod, U., Burjánek, J. & Fäh, D., 2019. Ambient vibration classification of unstable rock slopes: a systematic approach, *Eng. Geol.,* **249,** 198–217.

Konno, K. & Ohmachi, T., 1998. Ground-motion characteristics estimated from spectral ratio between horizontal and vertical components of microtremor, *Bull. seism. Soc. Am.,* **88**(1), 228–241.

Le Roux, O., Jongmans, D., Kasperski, J., Schwartz, S., Potherat, P., Lebrouc, V., Lagabrielle, R. & Meric, O., 2011. Deep geophysical investigation of the large Séchilienne landslide (Western Alps, France) and calibration with geological data, *Eng. Geol.,* **120**(1–4), 18–31.

Lévy, C., Baillet, L., Jongmans, D., Mourot, P. & Hantz, D., 2010, Dynamic response of the Chamousset rock column (Western Alps, France), **115**(F4),.

Lévy, C., Jongmans, D. & Baillet, L., 2011. Analysis of seismic signals recorded on a prone-to-fall rock column (Vercors massif, French Alps), *Geophys. J. Int.,* **186**(1), 296–310.

Mainsant, G., Larose, E., Brönnimann, C., Jongmans, D., Michoud, C. & Jaboyedoff, M., 2012. Ambient seismic noise monitoring of a clay landslide: toward failure prediction: seismic noise monitoring of a landslide, *J. geophys. Res.: Earth Surf.,* **117**(F1), F01030, doi:10.1029/2011JF002159 .

Michel, C., 2007. *Vulnérabilité Sismique de l'échelle du bâtiment à celle de la ville - Apport des techniques expérimentales in situ - Application à Grenoble*, PhD thesis.

Michel, C. & Guéguen, P., 2010. Time-frequency analysis of Transitory/Permanent frequency decrease in civil engineering structures during earthquakes, *Struct. Health Monitor.,* **9**(2), 159–171.

Moore, J.R., Gischig, V., Burjanek, J., Loew, S. & Fah, D., 2011. Site effects in unstable rock slopes: dynamic behavior of the Randa instability (Switzerland), *Bull. seism. Soc. Am.,* **101**(6), 3110–3116.

Panzera, F., D'Amico, S., Lotteri, A., Galea, P. & Lombardo, G., 2012. Seismic site response of unstable steep slope using noise measurements: the case study of Xemxija Bay area, Malta, *Nat. Hazards Earth Syst. Sci.,* **12**(11), 3421–3431.

Peterson, J.R., 1993. Observations and modeling of seismic background noise, USGS Numbered Series 93-322, U.S. Geological Survey, Code Number: 93-322, Open-File Report.

Poggi, V., Ermert, L., Burjanek, J., Michel, C. & Fäh, D., 2014. Modal analysis of 2-D sedimentary basin from frequency domain decomposition of ambient vibration array recordings, *Geophys. J. Int.,* **200**(1), 615–626.

Reynaud, J.-Y., Ferrandini, M., Ferrandini, J., Santiago, M., Thinon, I., André, J.-P., Barthet, Y., Guennoc, P. & Tessier, B., 2013. From non-tidal shelf to tide-dominated strait: the Miocene Bonifacio Basin, Southern Corsica, *Sedimentology,* **60**(2), 599–623.

Vella, A., Galea, P. & D'Amico, S., 2013. Site frequency response characterisation of the Maltese islands based on ambient noise H/V ratios, *Eng. Geol.,* **163,** 89–100.

Wathelet, M., Chatelain, J.-L., Cornou, C., Giulio, G.D., Guillier, B., Ohrnberger, M. & Savvaidis, A., 2020. Geopsy: a user-friendly open-source tool set for ambient vibration processing, *Seismol. Res. Lett.,* **91**(3), 1878–1889.

## APPENDIX A: INDIVIDUAL POWER SPECTRAL DENSITIES

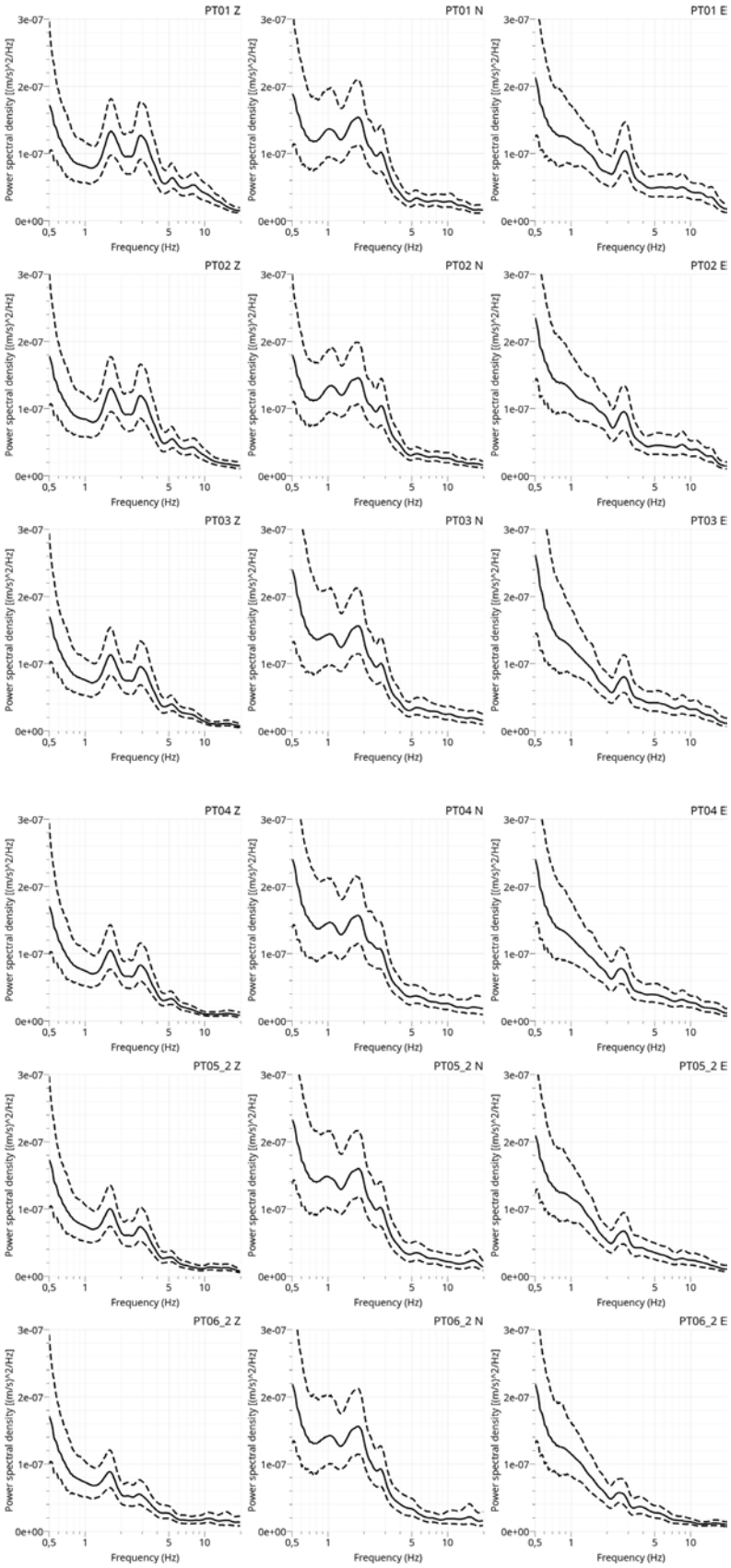


**Figure A1.** PSD of 3 hr of ambient vibrations (windy day) in the three components of motion from stations 01 (seaside) to 06. Mean (solid line) and standard deviation (dashed lines).

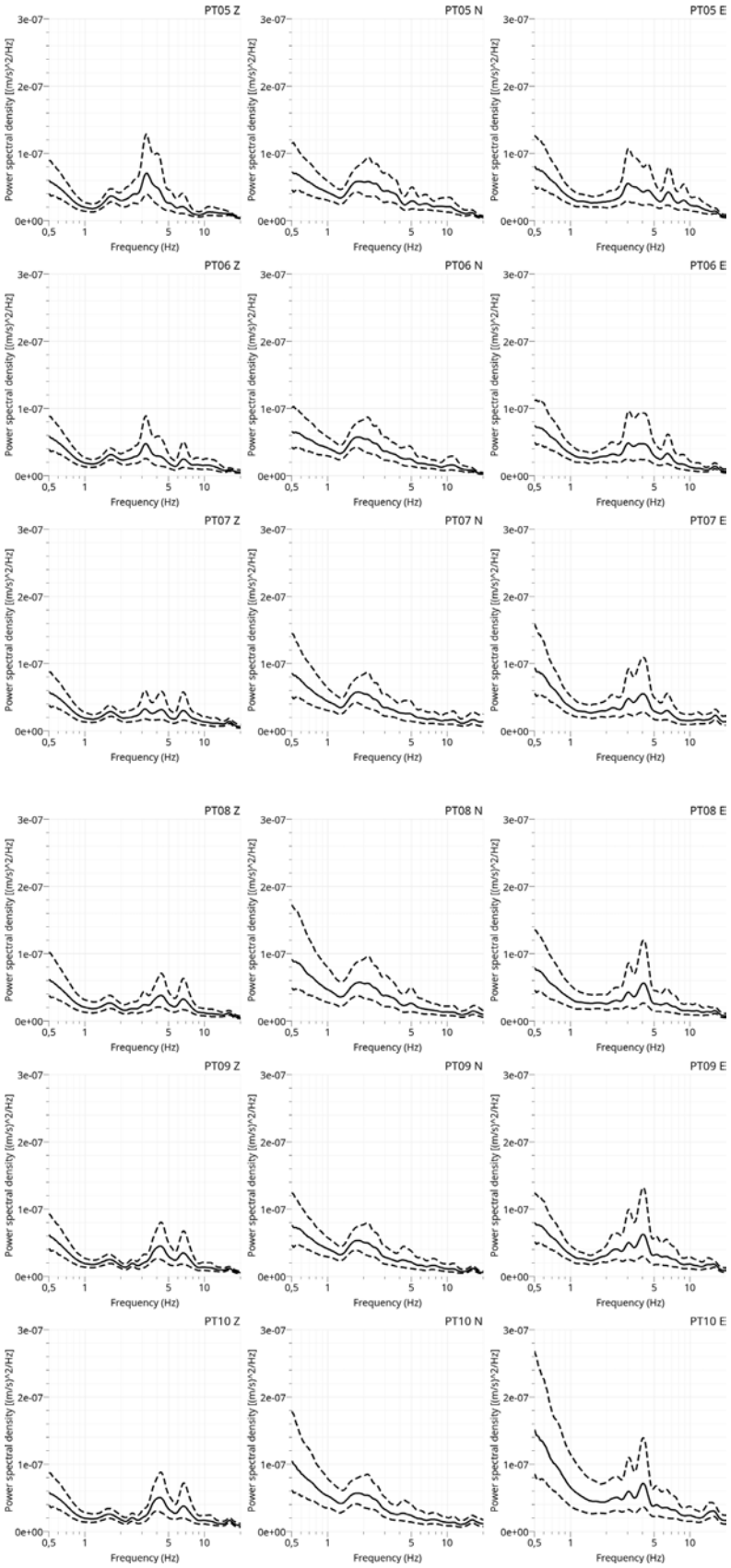


**Figure A2.** Power spectral density of 3 hr of ambient vibrations (calm day) in the three components of motion from stations 06 to 10 (harbour side). Mean (solid line) and standard deviation (dashed lines).